Hindawi
Advances in Meteorology
Volume 2023, Article ID 1175426, 20 pages
https://doi.org/10.1155/2023/1175426

Research Article

The Synergic Effects of Climate Variability on Rainfall Distribution over Hare Catchment of Ethiopia

Abebe Temesgen Ayalew

Water Technology Institute, Arba Minch University, Arba Minch, Ethiopia

Correspondence should be addressed to Abebe Temesgen Ayalew; abebe.temesgen@amu.edu.et

Received 17 December 2022; Revised 4 October 2023; Accepted 16 October 2023; Published 6 November 2023

Academic Editor: Mojtaba Nedaei

Climate analysis at relevant time scales is important for water resources management, agricultural planning, flood risk assessment, ecological modeling, and climate change adaptation. This study analyzes the spatiotemporal variability of climate on rainfall distribution for the Hare catchment of Ethiopia. Numerous hydroclimatic variables and scenarios were developed to assess the pattern of rainfall during different seasons. The average annual precipitation varies between −37.3%, +33.1%, and −38.2%, +61.2%, for RCP 4.5 and RCP 8.5, respectively. The anticipated declines in mean seasonal rainfall changes for the Bega and Belg seasons range from −69.6% to 88.4% and from −60.6% to 15.2% for RCP 4.5 and RCP 8.5, respectively. Climate models predict that the average periodic precipitation considered for the Kiremt season will vary from −12.1% to 1.33%. The Belg, Kiremt, and Bega seasons will likely see a 28.2%, 12.2%, and 22.6% drop in mean seasonal precipitation, respectively. The decrease in stream flow accompanied by the aforementioned climate scenarios (RCP 4.5 and RCP 8.5) can be as high as 19.6% and 6.7%, respectively. Also, the amount of discharge will reduce in the near future because of a substantial reduction in rainfall and a rise in evapotranspiration in the catchment. This decline in stream flow has its own effect on the future availability of water resources. The research finding is vital to environmental protection authority, decision makers, and scientific community to undertake climate change adaption techniques for rain scare areas. A program combined with multi-RCMs to evaluate climate change effects on hydrometeorology generated a novel approach to this research with appropriate adaptation mechanisms.

1. Introduction

Global warming due to climate change is one of today's most persistent problems. It has effects on the lives of people, property, the ecosystem health and services, land use/cover, watershed hydraulics, and large-scale water/groundwater resources [1–3]. Most scholars suggested that the climate change effect was mostly manifested by an increase in global temperature. In developing countries such as Ethiopia, the effect of precipitation is high as compared to temperature [4]. The amount of rainfall is an indication of climate change since rainfall has a direct effect on the environment and is associated with the growth of the country's economy [5]. The usual form of precipitation in Ethiopia is rainfall. The agricultural activities of a certain country also depend on the amount of rainfall, which is very important in this regard.

The existence of a huge population in developing countries such as Ethiopia requires a detailed investigation of the variability of rainfall and its trend. In addition to this natural calamity, there will be, for instance, floods and droughts due to uneven distribution of rainfall. Hare catchment, the catchment found near Arba Minch city, was the susceptible region with the aforementioned problem. In the past, in 2001, 2007, 2013, and 2019, the surrounding areas of the catchment were extremely agonized by this problem, and in the year 2013, the highest flood enormity of 60–120 cm was recorded with the resettlement of around 60 households from their residence. Similar situations have happened in different parts of the world. Excessive rainfall caused flooding, for instance, in Kendari, which is one of the cities in Indonesia, where most of the time floods happened, and historically, around 19 flood events were documented

from 2000 until 2017. Also, another city in Indonesia, Palu, suffered from similar circumstances, and in 2012, a huge magnitude of floods affected a lot of people [6–8]. For best prediction and reliability purposes, most of the time, the annual rainfall data are preferred to the mean value [9–15]. The research focuses on inspecting the uneven distribution of yearly as well as monthly precipitation for a record period of 30 years in the Hare catchment of Ethiopia. The data were utilized to explain which kinds of rainfall experienced significant variations as a consequence of the changing climate. Also, the authors in [16] provide the appropriate portion of the study's findings. This paper aims to be used as a guide for comprehensive rainfall investigations and basic investigations of climate variation's impact on diverse forms of rainfall to come in subsequent rainfall and environmental change studies. The present research applied a bias-corrected MME to nine GCMs [17]. This helps to examine the erraticism of precipitation under historical and upcoming weather conditions. The RCA4 RCM was selected while, in conjunction with the CORDEX project, and it downscaled an enormous amount of GCMs for Africa, indicating a desire to examine the effectiveness of the GCMs in downscaled scenarios compared to measured or actual data. The research site is recognized as the cultivated endowed regions, plus extensive hydraulic structures or schemes for growing agricultural crops are presently ongoing. In addition, the region's growing population drives up the consumption of water. Therefore, it is essential to keep track of the region's water supply. A multi-RCM approach was employed in the current research for evaluating the impact of climate variability on hydrometeorology, including recently demonstrated emission pathway predictions that will enhance the nation's adaptation strategy. The study encompassed the following specific objectives in our study to accomplish this main aim: (i) efficiency evaluation of the regional climate model; (ii) pattern identification for metrological and hydrological parameters; (iii) calibration and validation of the hydrological model; and (iv) sensitivity analysis of model parameters. In addition, by illustrating how to utilize RCMs in development attempts, this research is likely to be highly helpful to future scholars. The anticipated rainfall and temperature outcomes from five bias-corrected GCMs have been determined with two common conditions, namely, RCP4.5 and RCP8.5 [18, 19]. The study's findings are analyzed and compared to those of prior studies [20, 21] in the same and nearby catchments. The findings might aid in the expansion of adequate adaptable strategies for proper water administration to make timely choices in response to the possible impact of changes in climate.

2. Methodology

2.1. Study Area Description. Hare catchment is a subcatchment of the Abaya Chamo subbasin, southern Ethiopia, with an enclosed coverage of 187.14 km^2. The catchment is generally located at 6°4′00″ and 6°17′30″ N latitudes and 37°27′00″ to 37°45′00″ E longitudes (Figure 1). Hare catchment is classified as steep valleys upstream and gradually becomes a flat river plain till it joins Lake Abaya [22].

2.2. Data Collection and Analysis

2.2.1. Time Series Metrological Data. Ethiopian National Meteorological Agency (ENMA) is an essential source for metrological data designed for the Hare catchment from 1987 to 2021, or about 30 years of data. Three climate data recording sites were situated nearby and surrounding the study area (Table 1). When comparing the availability of data for each station, one station has more available data than the others. Chencha and Dorze stations only offer rainfall and temperature data (Table 1). But the Arba Minch gauging station (synoptic station) was utilized to provide additional meteorological data for other stations. Arba Minch's weather is much different from that of Chencha and Dorze.

2.3. Spatial and Temporal Data

2.3.1. Digital Elevation Model. The resolution of the DEM is determined by the size of each cell. On December 15, 2022, https://asf.alaska.edu/ provided a 12.5 m × 12.5 m resolution DEM for the Hare catchment (Figure 2). The obtained DEM grids were mosaicked with ArcGIS 10.1 software and utilized in the SWAT model to delineate catchments and for further analysis.

2.3.2. Land Use/Cover Data. In Ethiopia, rain-fed agriculture is the most widely employed traditional farming technique. Land use land cover can have a considerable impact on land surface sediment erosion. Vegetation cover can mitigate the effect of precipitation on soil erosion. Changes in land cover, such as the conversion of thick forest to agricultural land, have accelerated erosion and increased sediment output at catchment outlets [23]. The Hare catchment is mostly occupied by modestly farmed terrain, with some forestland in the higher reaches. The lowest half of the catchment has heavily farmed land and shrub vegetation. The study region also features a high concentration of riparian vegetation. The study catchment is dominated by highly farmed, moderately cultivated, and shrub regions (Figure 3).

2.3.3. Soil Data. The soil type has a certain factor for the runoff generation as well as the infiltration capacity of the catchment [24]. After overlaying clipped study area map to the Ethiopian soil map the classified major soil type of the catchment are easily identified and listed as follows: eutric nitisols dystric nitisols, orthic acrisos, eutric fluvisols, and dystric fluvisols (Figure 4).

2.4. Setup for SWAT Model

2.4.1. Delineation of Catchment. Arc Map interface voguish ArcGIS 10.1 was used to manage and interpret geographic data that were utilized as input for SWAT. Catchment delineation is the first stage in starting a SWAT model catchment simulation. SWAT allows users to designate catchments and subcatchments utilizing DEM to perform sophisticated GIS tasks to assist users in splitting catchments

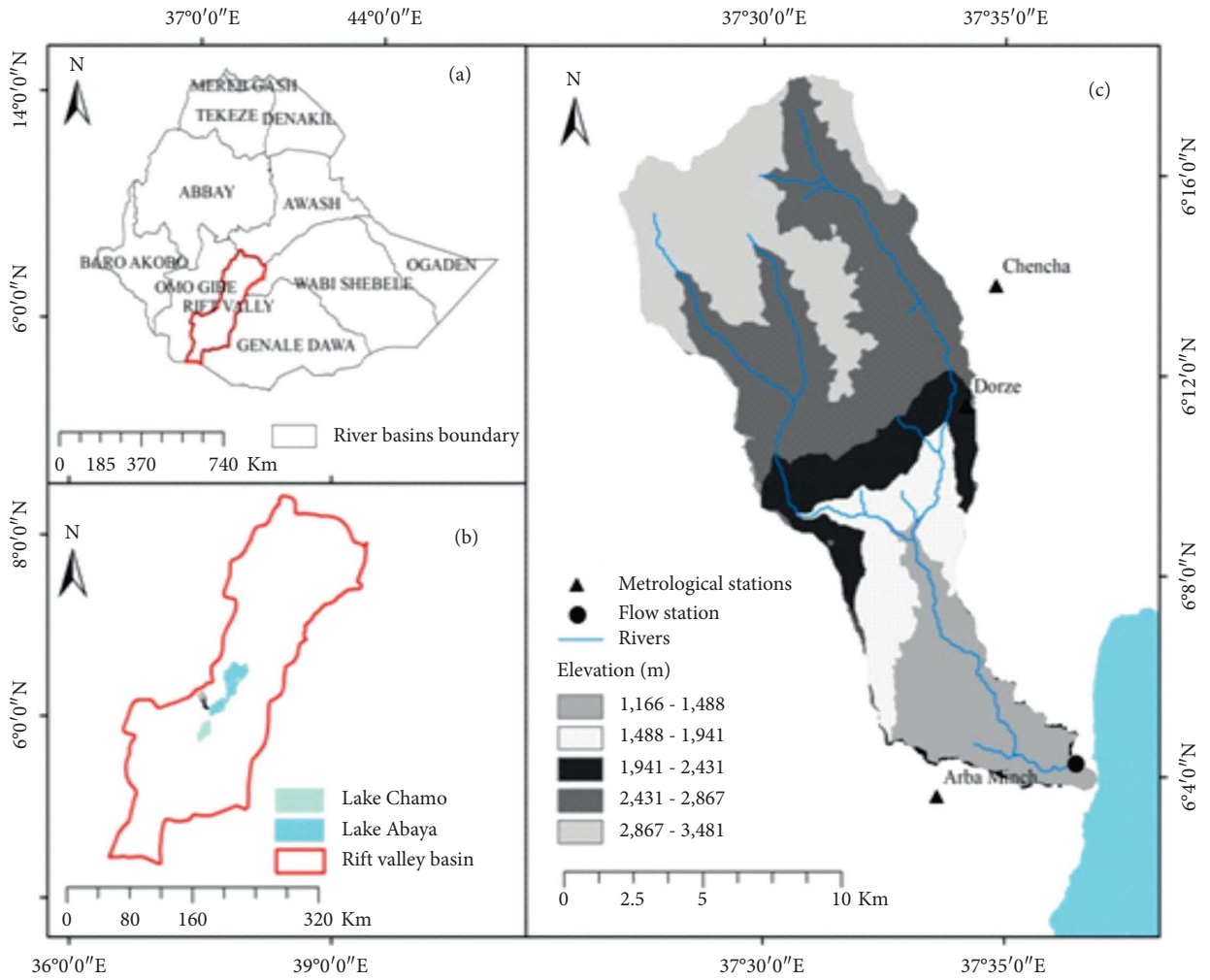

Figure 1: (a) Ethiopian major river basins; (b) Rift valley lake basin; and (c) Hare catchment.

into numerous hydrologically related subcatchments for use in SWAT catchment modeling [25]. During the delineation of catchments and subcatchments, the Hare catchment was defined with an outflow point at the catchment's outlet. The ArcGIS was enhanced by using a catchment delineation tool. Catchment delineation was performed by SWAT model. The model created the stream network in place of the entire digital elevation model by utilizing the concepts of direction and accumulation of flow. The smaller threshold area revealed greater drainage network information, as well as a significant number of subcatchment and HRU. This, however, necessitates additional processing time and a considerable amount of computer space. For this study, a threshold area of 540 ha was used, and the catchment outflow was manually inserted and selected before concluding the catchment delineation. The model then defined a 187.14 km^2 catchment with 19 subcatchments (Figure 5).

2.4.2. Analysis of Hydrologic Response Unit (HRU). HRUs are subcatchment regions that have a distinct land use/cover, soil, and slope combination. HRUs can be assigned to each subcatchment by assigning only one HRU based on the major spatial data combinations. A multiple HRU analysis option was employed for this investigation. SWAT land use datasets have four-letter codes established in the GIS interface (Figure 6). To connect the land use map to the SWAT database, the lookup table in the SWAT was prepared in a way that was consistent with the loading of the land use/cover map.

By loading lookup table, the soil layer on the geographical map was connected and stored in the database. To incorporate this map into the model, a user-defined soil database which includes physical as well as chemical characteristics of each soil was created and amalgamated together with the combined lookup table. The provided soil map's categories of soil have been encoded using a lookup table (Figure 7).

Furthermore, to land use and soil, HRUs have been categorized by slope classification. The multiple slope approach tends to be desired when considering number slope categories for HRU definitions. In the present investigation, a lot slope alternatives were selected and the slope class has

Table 1: Summary of availability of metrological data.

No	Recorded stations	Latitude (m)	Longitude (m)	Elevation (m)	Elements					
					Maximum temperature	Minimum temperature	Rainfall	Sunshine hour	Wind speed	Relative humidity
1	Arba Minch	340637.01	670048.55	1207	√	√	√	√	√	√
2	Chencha	342900.72	688840.67	2632	√	√	√	N/A	N/A	N/A
3	Dorze	341782.21	684420.58	2505	√	√	√	N/A	N/A	N/A

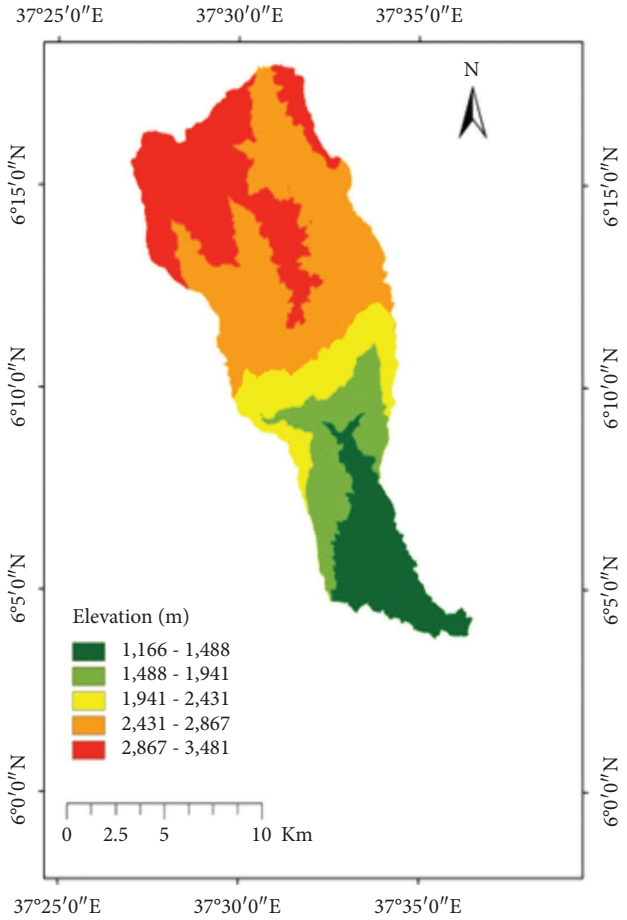

Figure 2: DEM of Hare catchment.

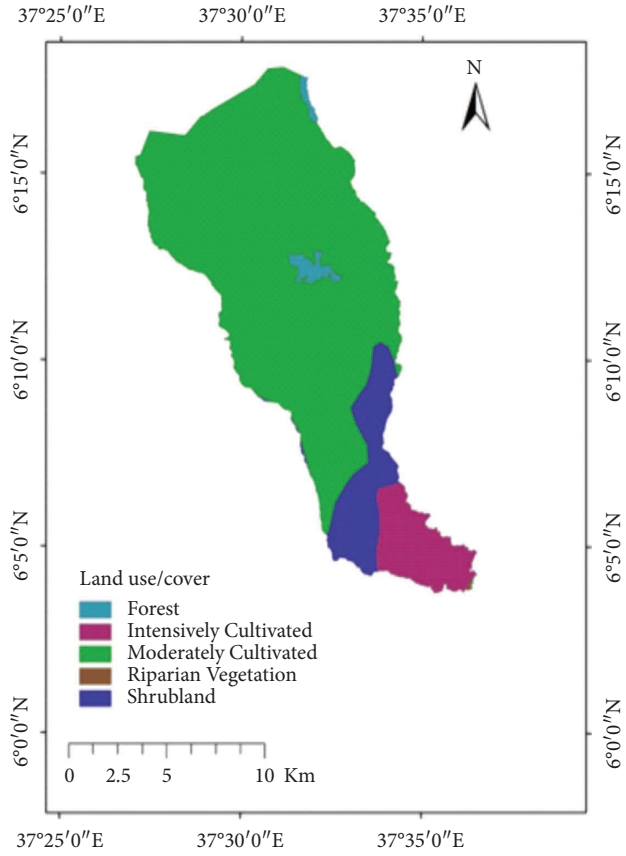

Figure 3: Land use/cover map of Hare catchment.

been divided into four classes with slopes that ranged from 0–3% to 3–6%, 6–12% to over 12% (Figure 8).

Following redefining the spatial structure, entirely of the aforementioned corporeal characteristics was layered on top for HRU definition. As stated by [26], the percentage of land use, soil and slope is 20%, 10%, and 10%, respectively, for the majority purposes of modeling. Small land use, soil, and slope classes inside a specific subcatchment could be dominant over close to significantly larger physical characteristics throughout HRU identification under specific threshold scales. The HRU in the present research was established by a 10%, 5%, and 5%, respectively. In the end, 77 HRUs for 19 small catchments were established alongside the whole Hare catchment HRU map (Figure 9).

2.4.3. Weather Data Definition

(1) Weather Generator. The precipitation statistical analysis model (PCP STAT) produced by the weather generator was used for the statistical analysis of everyday rainfall records required for creating climate files. The dew point (dew02) is a configurable value for the weather generator. As stated by [20], dew02 is used for calculating the daily mean metrological data. Angstrom–Prescott empirical equation (21) was applied for converting existing sunlight hour into solar radiation. Weather observatories were placed using latitude, longitude, and elevation measurements.

2.4.4. Model Sensitivity, Calibration, and Validation. The model's appropriateness aimed at the intended purpose ought to be assessed by sensitivity analysis, standardization (calibration), and justification (validation) [22]. The calibration process involves altering the input variables and comparing anticipated results with actual results till the target function is achieved, and the calibration is carried out by using automatic calibration. Nevertheless, in the present investigation, an automated calibration approach was used for calibration from 1990 to 2001 and validation from 2002 to 2007, with a two-year warm-up phase from 1988 to 1989. The calibrated model was evaluated in contradiction of a self-determining set of observed data in order to be used for measuring sediment production. The capacity should be treated as sound in simulation stages of the evaluation [27]. Model performance was evaluated by visual inspection of hydrographs value and with combination of objective functions.

2.4.5. Model Performance Evaluation. A model's accuracy, consistency, and flexibility must all be considered. To evaluate the model's performance, a forecast efficiency

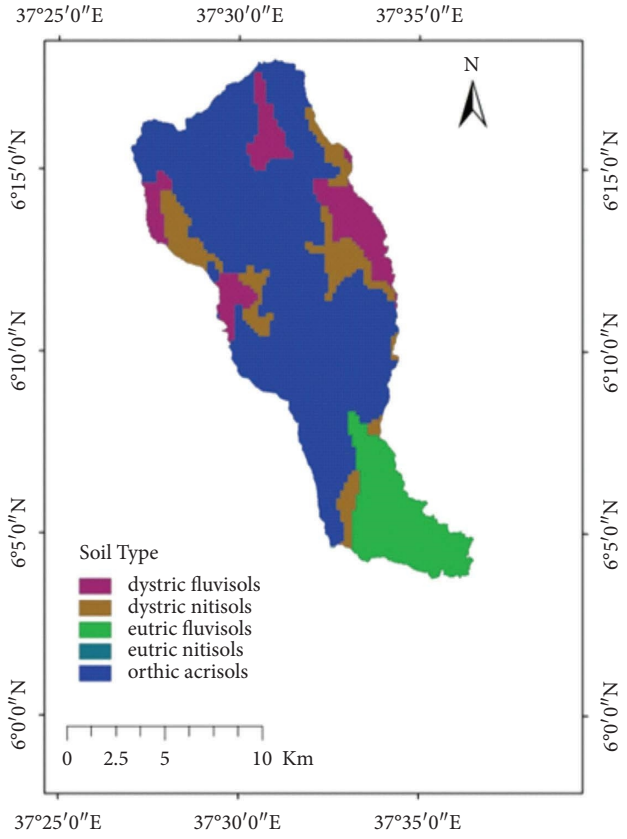

Figure 4: Soil map of Hare catchment.

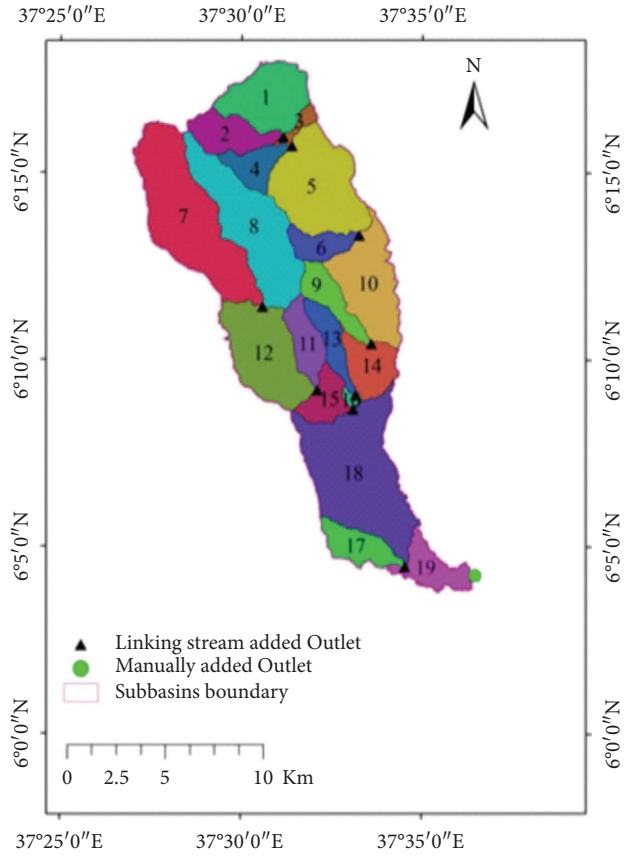

Figure 5: Delineated Hare catchment and subcatchments with their code numbers.

criterion is required. Assessing the efficacy of a hydrologic model necessitates subjective and/or objective judgments of the model's simulated behavior's proximity to data [23]. In this study, the model's performance is evaluated by the following points.

(1) Nash–Sutcliffe Efficiency (ENS). It helps to judge the fit concerning the outcome of the model and actual measured hydrograph shapes. The effectiveness of the model is determined by ENS as described in the following equation:

$$E_{\mathrm{NS}} = 1 - \frac{\sum_{i=1}^{n}\left(q_{oi} - q_{si}\right)^2}{\sum_{i=1}^{n}\left(q_{oi} - \overline{q}_o\right)^2}. \tag{1}$$

ENS can range between 1 and $-\infty$ and operates best when it is one. Values ranging from 0.80 to 0.90 suggest that the model works very well, whereas values ranging from 0.90 to 1 designate that the model performs exceptionally well [24].

(2) Coefficient of Determination (R^2). R^2 reflects the model approach to recreate the observed value through a given time period and for a given time step. R^2 values vary from 1.0 (best) to 0.0.

$$R^2 = \frac{\left[\sum_{i=1}^{n}\left(q_{si} - \overline{q}_s\right)\left(q_{oi} - \overline{q}_o\right)\right]^2}{\sum_{i=1}^{n}\left(q_{si} - \overline{q}_s\right)^2 \sum_{i=1}^{n}\left(q_{oi} - \overline{q}_o\right)^2}. \tag{2}$$

The predisposition of anticipated threshold higher/smaller than measured value is assessed by percent bias (PBIAS) [25]. The absolute value of PBIAS should be as low as possible for a well-performing model. The PBIAS is provided by the following equation:

$$\mathrm{PBIAS} = \left[\frac{\left(\sum_{i=1}^{n} q_{si} - \sum_{i=1}^{n} q_{oi}\right)}{\left(\sum_{i=1}^{n} q_{Oi}\right)}\right] * 100. \tag{3}$$

(3) The Ratio of Root Mean Square Error to Observation Standard Deviation (RSR). It serves as an error index indicator. RSR has a value between zero and one, with the lower value, closer to zero, suggesting better model representation and one indicating poor model performance.

$$\begin{aligned}\mathrm{RSR} &= \frac{\mathrm{RMSE}}{\mathrm{STDEV}_{\mathrm{ob}}} \\ &= \frac{\sqrt{\sum_{i=1}^{n}\left(q_{oi} - q_{si}\right)^2}}{\sqrt{\sum_{i=1}^{n}\left(q_{oi} - \overline{q}_s\right)^2}},\end{aligned} \tag{4}$$

where q_{si} is the simulated discharge (m^3/sec), q_{oi} is the measured discharge (m^3/sec), $\overline{q}_s$ is the average simulated discharge (m^3/sec), and $\overline{q}_o$ is the average measured discharge (m^3/sec).

2.4.6. Soil and Water Assessment Tool (SWAT). SWAT model is a physically based, semidistributed, long-term simulation, deterministic, and originated from agricultural

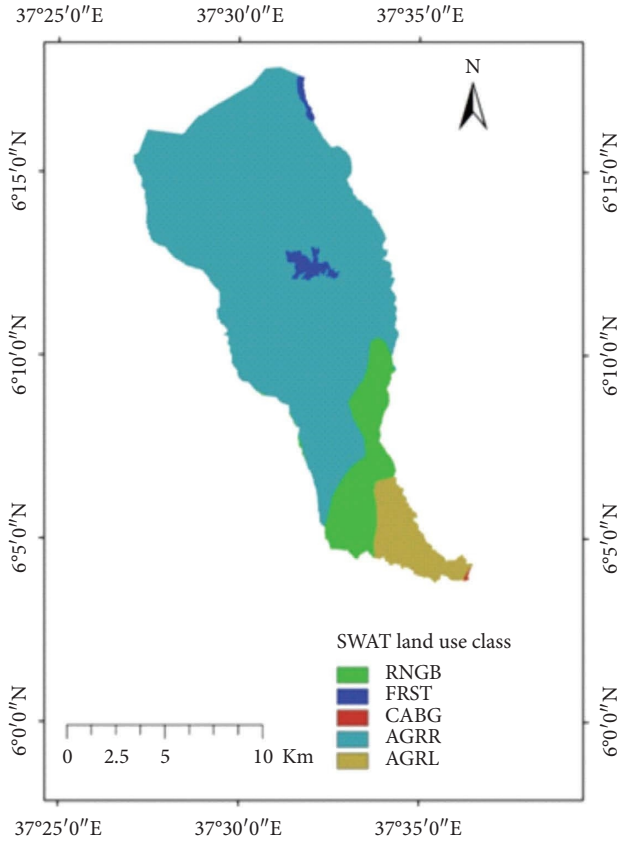

Figure 6: SWAT model reclassified land use code.

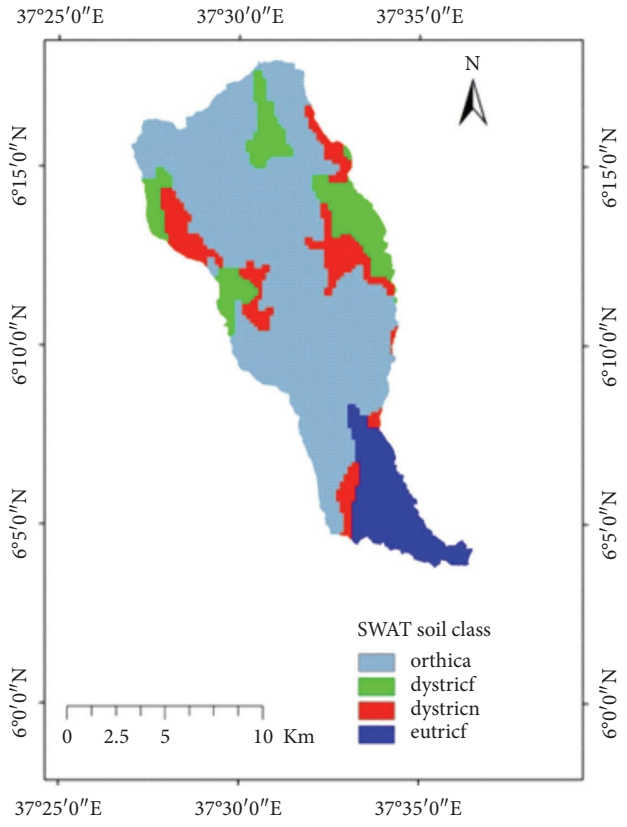

Figure 7: SWAT database soil reclassification.

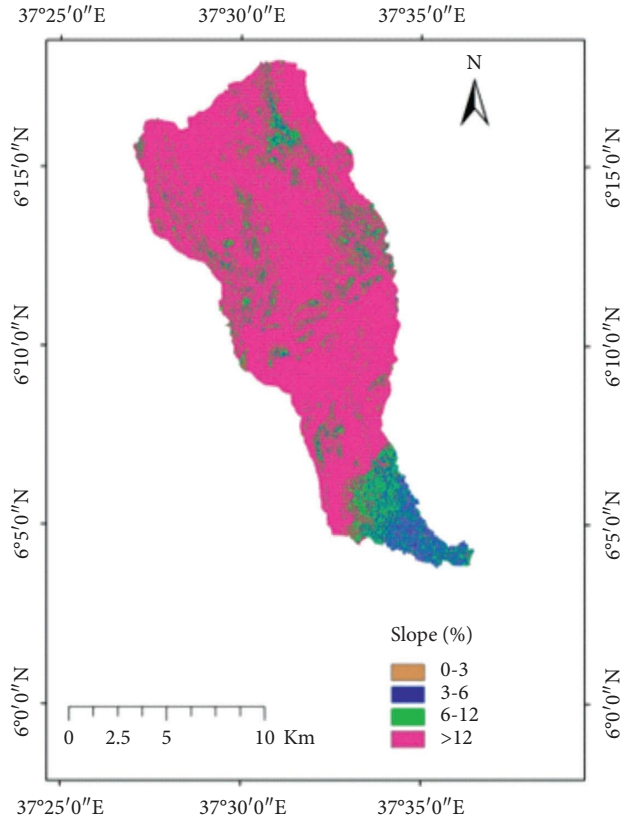

Figure 8: Reclassified slopes for Hare catchment by SWAT model.

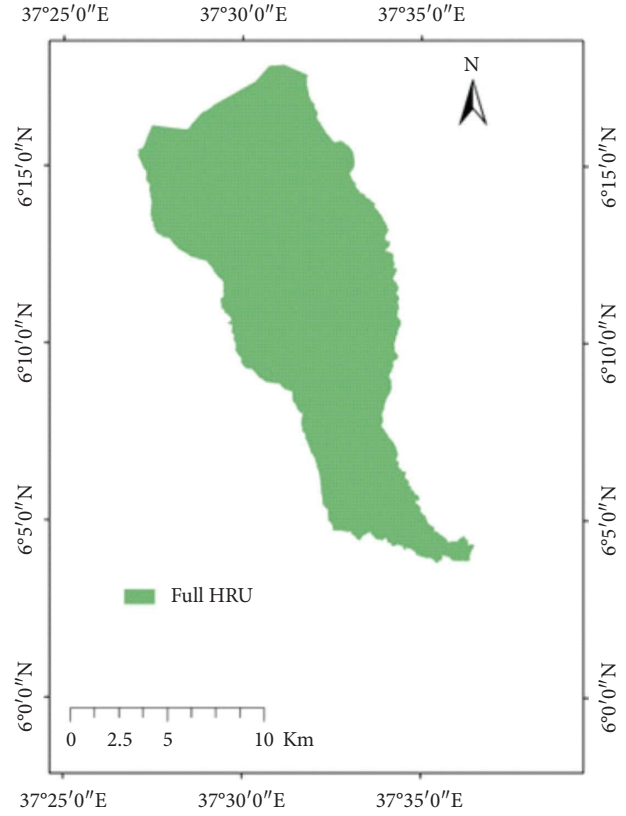

Figure 9: Full hydrologic response unit (HRU) map of the Hare catchment.

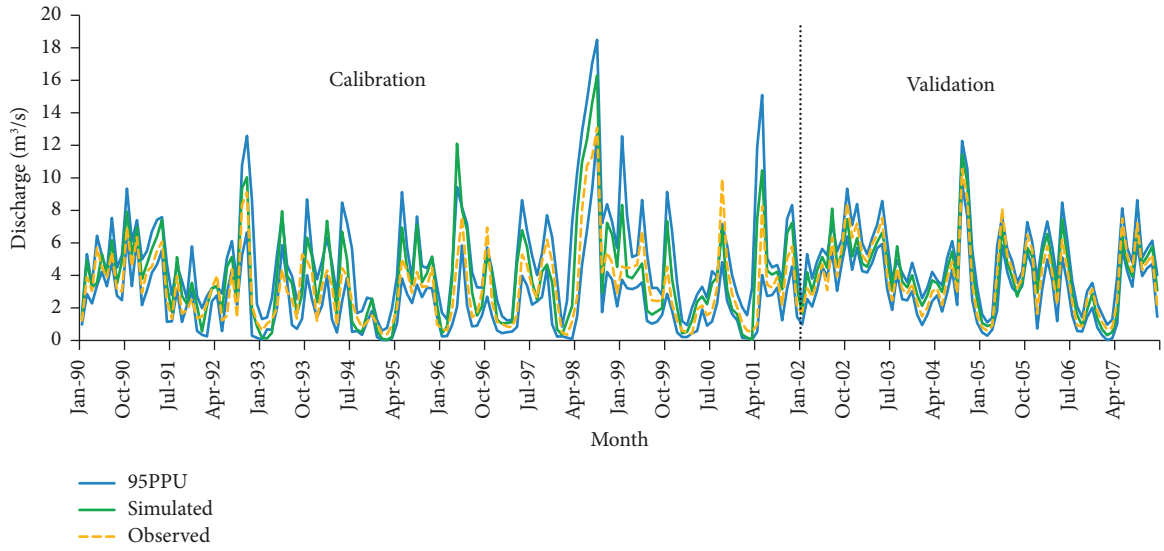

Figure 10: For calibration and validation, a monthly observed and simulated hydrograph.

models with spatially distributed parameters and operating on a daily time [26]. SWAT model has been used worldwide and considered as adaptable environmental model that can be used to evaluate the biophysical impacts of intensification of interventions at the watershed scale, which supports more effective watershed management and the development of better informed policy [28, 29]. The model has been widely applied for the simulation of runoff, sediment yield, nitrogen, and phosphorus losses from watersheds in different geographical locations, with varying soils, land use, and management conditions over long periods of time. Several researchers for instances, the authors [30] were proved the applicability of SWAT model in the Ethiopian watersheds.

2.4.7. Description of Regional Climate Model. In this study, projected climate datasets were used. Datasets with a grid spacing of 0.44° 0.44° (50 km × 50 km) were accessed from the CORDEX-Africa database at https://cordexesg.dmi.dk/esgf-web-fe/. The reference period for the analysis was from 1986 to 2005, and the future midterm period was chosen between 2051 and 2080 to match the timeframes typically utilized in studies of climate change. Basic climatological information including precipitation, maximum and minimum temperatures, solar radiation, wind speed, and relative humidity are included in this climate model's output for both the reference and future periods. The climate effect assessment was conducted using the extreme (RCP 8.5) and the intermediate (RCP 4.5) emission scenarios for the midterm era (the 2050s). In the present study, seven regional climate model datasets were employed.

2.4.8. Evaluation of CORDEX RCMs. By plotting the actual and simulated data for the yearly cycle and interannual variability, the CORDEX rainfall simulations were evaluated using statistical performance indicators. The analysis was carried out using a statistical technique for evaluating model performance that encompasses bias, root means square error (RMSE), Pearson correlation coefficient, and coefficient of variation (CV) and is discussed in the following sections [31].

$$\begin{aligned}
\text{Bias} &= 100 * \frac{\overline{R}_{\text{rcm}} - \overline{R}_{\text{obs}}}{\text{R}_{\text{obs}}} \\
\text{RMSE} &= \sqrt{\frac{\sum_1^N (R_{\text{rcm}} - R_{\text{obs}})2}{\text{N}}} \\
\text{Correl} &= \frac{\sum_{t=1}^{n} (R_{\text{rcm}} - \overline{R}_{\text{obs}})(R_G - \overline{R}_G)}{\sqrt{\sum_{t=1}^{N} (R_{\text{rcm}} - \overline{R}_{\text{rcm}})2} \sqrt{\sum_{t=1}^{N} (R_G - \overline{R}_G)2}} \\
\text{CV} &= 100 * \frac{\sigma_R}{R},
\end{aligned} \tag{5}$$

where the R bar represents the mean value of rainfall in the analysis period; R is the average rainfall in the basin in a given year; rcm is a subscript for the regional climate model, while G refers to a subscript for rainfall values obtained from the rain gauge network.; σ is the standard deviation. The RCMs used in this study are the Canadian Regional Climate Model CanRCM4, KNMI Regional Atmospheric Climate Model, Version (RACMO22T), SMHI Rossby Center Regional Atmospheric Model (RCA4), MPI regional model (REMO), CLMcom COSMO-CLM (CCLM4), and CLMcom COSMO-CLM (CCLM4).

2.4.9. Bias Correction. Bias correction for rainfall and temperature was made using the CMhyd tool with the nearest grid of RCM data. Researchers have utilized a variety of bias correction techniques to eliminate bias from climate model data [32]. For this study, the distribution mapping

technique was used to correct bias in the dynamically downscaled temperature and precipitation data. Teutschbein and Seibert (2012) went into greater detail about the techniques. On the other hand, the mean-based bias adjustment approach was used to correct a bias for RCM simulation of future relative humidity, wind speed, and solar radiation [33]. Equation (6) provides the mean-based bias correction method used in this study.

$$X_{\text{adj}} = X_{\text{rcm,future}} + \left(\overline{X}_{\text{obs,hist}} - \overline{X}_{\text{rcm,hist}}\right), \quad (6)$$

where X_{adj} = adjusted data; X_{rcm}, future = RCM future data; and $\overline{X}_{\text{obs,hist}}$ and $\overline{X}_{\text{rcm,hist}}$ are the mean for observed and RCM data, respectively.

3. Results

3.1. SWAT Model Calibration and Validation

3.1.1. Stream Flow Calibration and Validation. The goal of the calibration procedure is to see if the simulated and observed flow values coincide by changing the sensitive model flow parameters within the specified range. For subsequent iterations in the calibration periods, the six more powerful (governing) flow characteristics are used as described in Table 2.

The validation procedure was also followed without altering the model flow parameters that had been altered during the calibration step. The model's performance was examined throughout the validation period (from January 1, 2002 to December 31, 2007).

According to Table 3, the model performed extremely well throughout the flow calibration and validation for calibration, $R^2 = 0.78$, ENS = 0.76, RSR = 0.57, and PBIAS = −12.5%, while for validation, $R^2 = 0.89$, ENS = 0.75, RSR = 0.44, and PBIAS = 10.2%. For calibration, the SUFI-2 uncertainty measure gave *P*-factors of 0.73 and *R*-factors of 0.42, and for validation, *P*-factors of 0.74 and *R*-factors of 0.52. This suggests that the 95% prediction of uncertainty (95PPU) band contains about 73% of calibration data and 74% of validation data, with *R*-factors of 0.42 and 0.52, respectively.

According to Figure 10, the maximum model output occurs in August 1998 for calibration and September 2004 for validation. Furthermore, the hydrographs (Figure 10) revealed that the model somewhat overstated flow in most years while underestimating flow in others. This means that the uncertainty analysis revealed that around 27% and 26% of the calibration and validation data, respectively, were questionable.

3.2. Assessment of Climate Change Impact

3.2.1. Baseline Hydroclimatic Variables. Figure 6 depicts the monthly patterns in maximum and lowest temperatures. Accordingly, February has the greatest maximum temperature (28.8°C) and July has the lowest (23.0°C), while March has the highest minimum temperature (13.1°C) and November has the lowest (10.4°C) (Figure 11).

As seen in Figure 12, the comparison of actual precipitation to GCM reference values. Similarly, in Figure 7, the highest significant variation between the MIROC5 baseline and the July values was 14 mm/month. The IPSL-CM5A-MR had the most substantial divergence in rainfall among all GCMs.

3.2.2. Temperature. Changes in the worldwide diurnal temperature range, DTR ($T_{\max}T_{\min}$), are an important indication of climate change [34]. We analyzed the DTR in the Hare catchment using the averages of the five GCMs for the baseline and future eras to study the significance of the variability of temperature as presented in Figure 13. Under all scenarios, the DTR will be smaller in the Kiremt and late Belg periods than in the baseline period, with just a slight difference in the beginning of the Belg season.

3.2.3. Rainfall. Figure 14 depicts percentage variations in expected rainfall on a seasonal and yearly basis for the near and distant future timeframes. The forecasts suggest that the Bega season will be longer, while the Belg and Kiremt seasons would be shorter. The estimated yearly rainfall loss varies from 6.5% (MPI-ESM-LR-RCP4.5) in the near future to 38.3% (CanEMS2-RCP8.5) in the distant future. CanESM2-RCP8.5 seasonal estimates indicate the greatest substantial declines in the Belg (55.2%) and Kiremt (51.5%) seasons. MPI-ESM-LR-RCP4.5 produced the lowest seasonal decreases of 8.5% in the Belg season and 11.2% in the Kiremt season.

3.2.4. Evapotranspiration. The current study's findings show that both emission scenarios enhance evapotranspiration. The spike is linked to the higher-than-expected temperature rise (Figure 14). Figure 15 depicts a steady increase in average annual and seasonal evapotranspiration rates across all scenarios. The anticipated annual average rise for RCP4.5 and RCP8.5 is 6.3–14.8% and 8.9–16.8%, respectively.

Figure 16 shows a strong connection between the monthly baseline stream flows predicted with various GCMs and the actual stream flow, with a coefficient value of roughly 0.89. There is, however, a difference between the observed and baseline periods. The highest difference is 7.8 mm/month achieved with the MIROC5 model in November, followed by 7.3 mm/month acquired with the IPSL-CM5A-MR in March. For the baseline period, the simulated stream flows with CanESM2 and IPSL-CM5A-MR are higher than the observed values, but with CSIRO, they are lower, except for January.

(1) Impact of Climate Change on Drought Characteristics. We examined the likelihood of drought incidence and mean drought index (SPI, RDI, and SDI) in the study area using an

Table 2: Summary of calibrated model flow parameters.

Parameters	Description	Range value	Calibration range	Fitted values	Rank
ALPHA_BF	Recession constant for alpha base flow	0-1	0-1	0.145	1
CANMX	High amount of canopy storage	0–10	0–10	2.688	2
CN2	Curve number for SCS runoff	35–98	±25%	0.126	3
SOL_Z	Soil depth (for each layer)	0–3000	0–3000	0.348	4
SURLAG	Lag time for surface runoff	0–10	0–10	9.586	5
GWQMN	Verge depth of water in the shallow aquifer	0–5000	0–5000	2374.738	6

Table 3: Indicators of model performance for monthly observed and simulated flow during calibration and validation (1990–2007).

Recording site	Simulation period	Uncertainty analysis		Model evaluation parameters			
		P-factor	*R*-factor	R^2	ENS	RSR	PBIAS
Hare @outlet point	Calibration (1990–2001)	0.73	0.42	0.78	0.76	0.57	−12.5
	Validation (2002–2007)	0.74	0.52	0.89	0.75	0.44	10.2

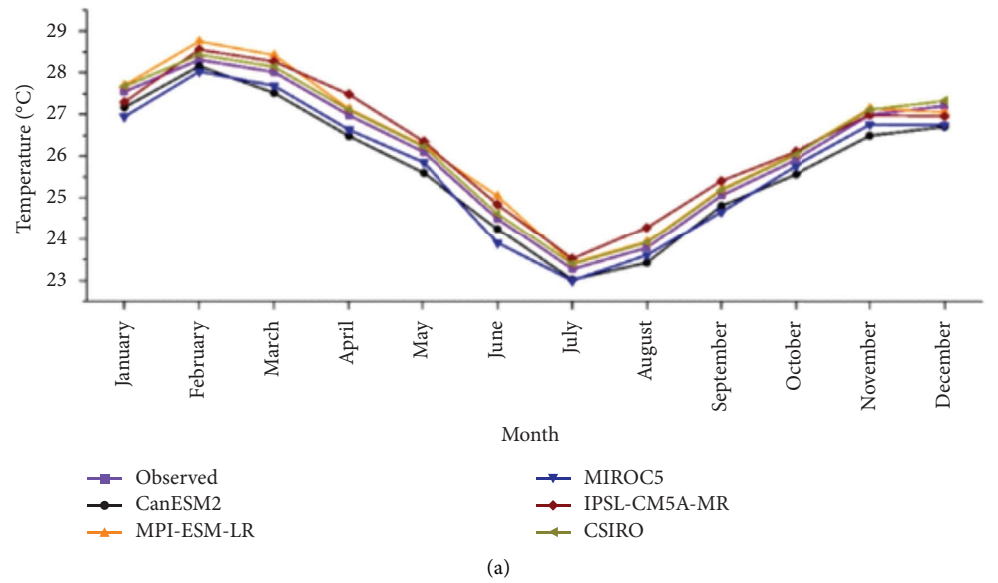

(a)

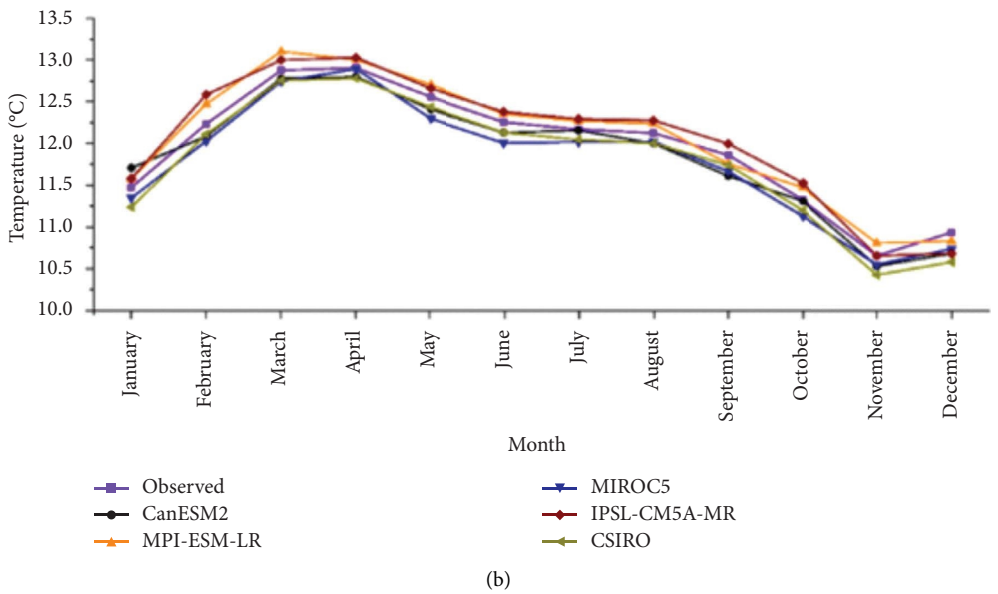

(b)

Figure 11: Monthly temperature observations and GCM simulations in the baseline period (1986–2005): (a) highest temperature and (b) lowest temperature.

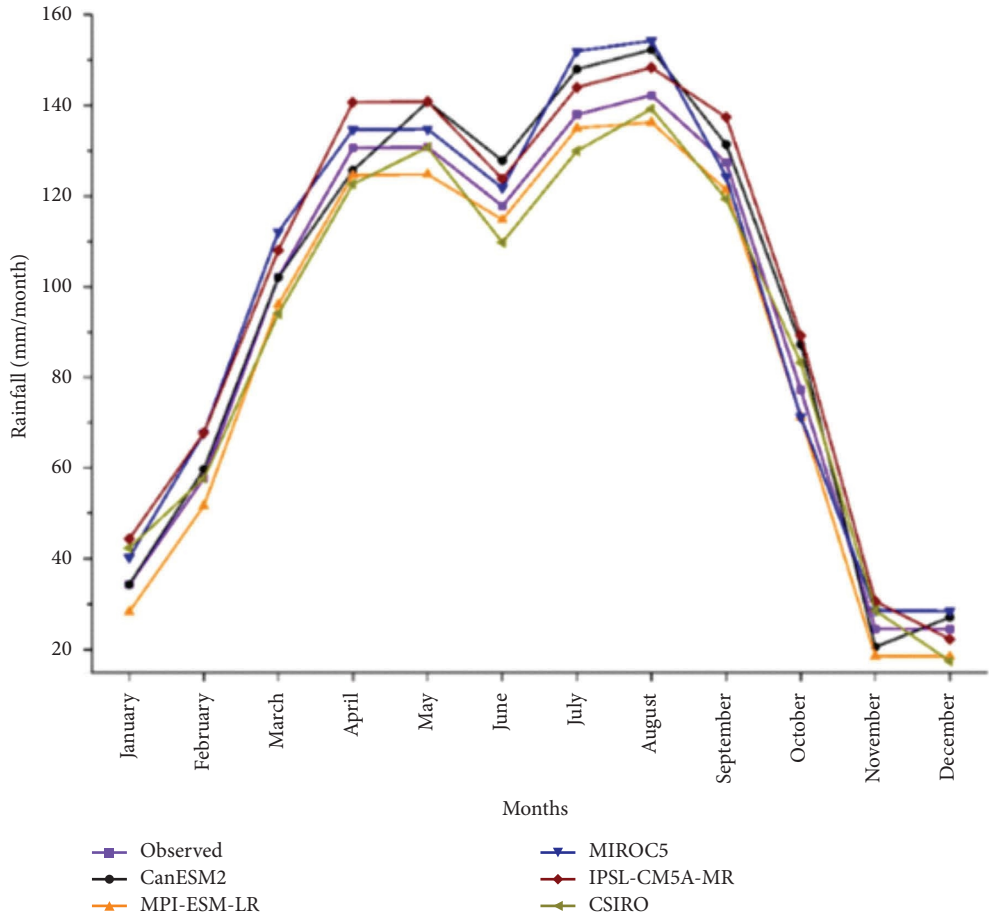

Figure 12: Observed monthly rainfall and GCM simulated baseline rainfall (1986–2005).

ensemble average of five GCMs for nearby and future periods under, RCP4.5 and RCP8.5 (Figure 17). The chance of drought incidence from January to December is calculated by dividing the number of years with a drought index value of 1 by the total number of years in the period [34]. Under RCP8.5, it reached its maximum (0.19) for the Belg (from February to May) in the distant future era (Figure 17(a)). This increased likelihood is mostly due to a considerable drop in predicted rainfall. Another cause might be the higher unpredictability of rainfall in Belgium. The SPI and RDI data demonstrated a similar temporal pattern of drought incidence (Figure 17(c)). This suggests that drought susceptibility is also strongly connected to the sorts of land use circumstances that may lead to available water shortages [35].

The probable function of the hydrological drought from the three indexes shows a value of 0.07 for the base line scenario and 0.14 for the predicted one. Figure 17 describes almost similar pattern for the three drought indexes. The output of this study also comparable with the scholars who put their own suggestion in upper blue Nile and Bilate catchment showed that the possibility of existence of metrological drought 0.22 and 0.16 in Belg and Kiremet, respectively [36, 37]. Also, the domain of existence of drought is manifested by the variability of climate especially rainfall over the area.

Figure 18 depicts the average mean monthly precipitation change of all individual RCMs over the research region for the midterm 2050s period. Climate model projections suggest that, with the exception of the CanRCM4 model, there will be a probable constant decrease in future rainfall quantity for virtually all months. The CanRCM4 model predicts a rise in rainfall quantity from January to September. The model projection for the base period is correct based on the data collection as shown in Figure 19.

Figure 19 depicts the expected midterm change in mean seasonal and annual rainfall for the Hare catchment related to the reference period. With rare exceptions, the anticipated changes in the basin's mean annual rainfall have showed

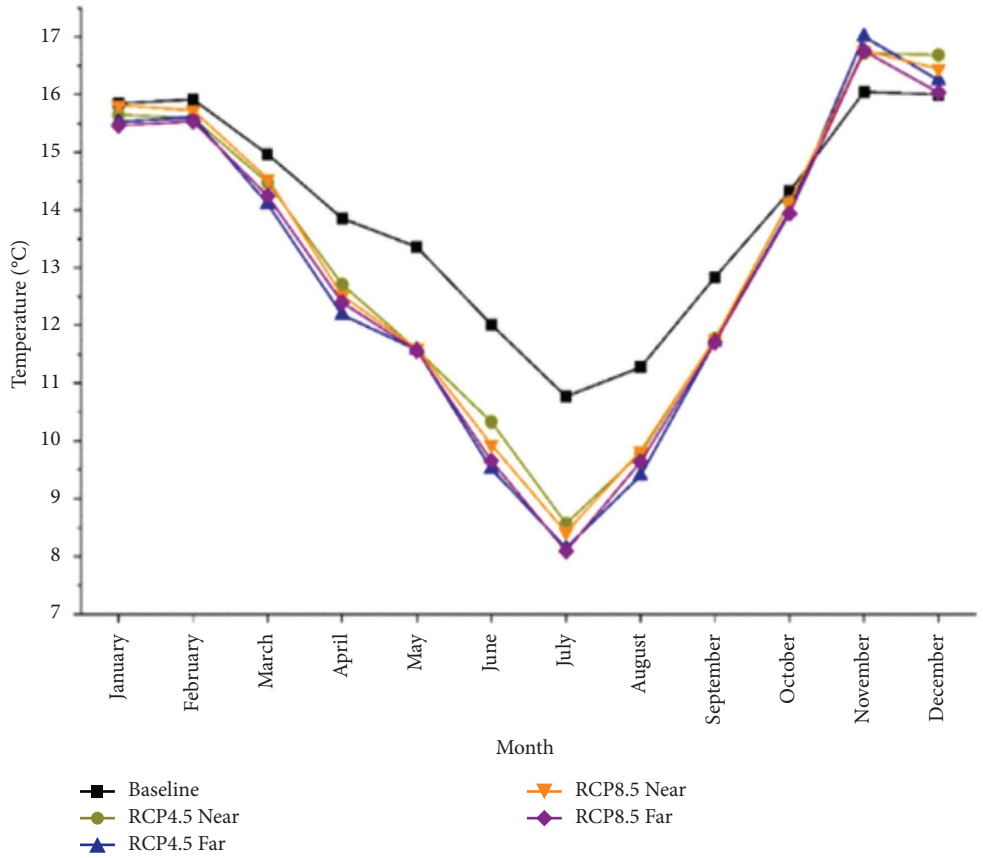

Figure 13: Diurnal temperature range (DTR) for the baseline, near, and far future periods.

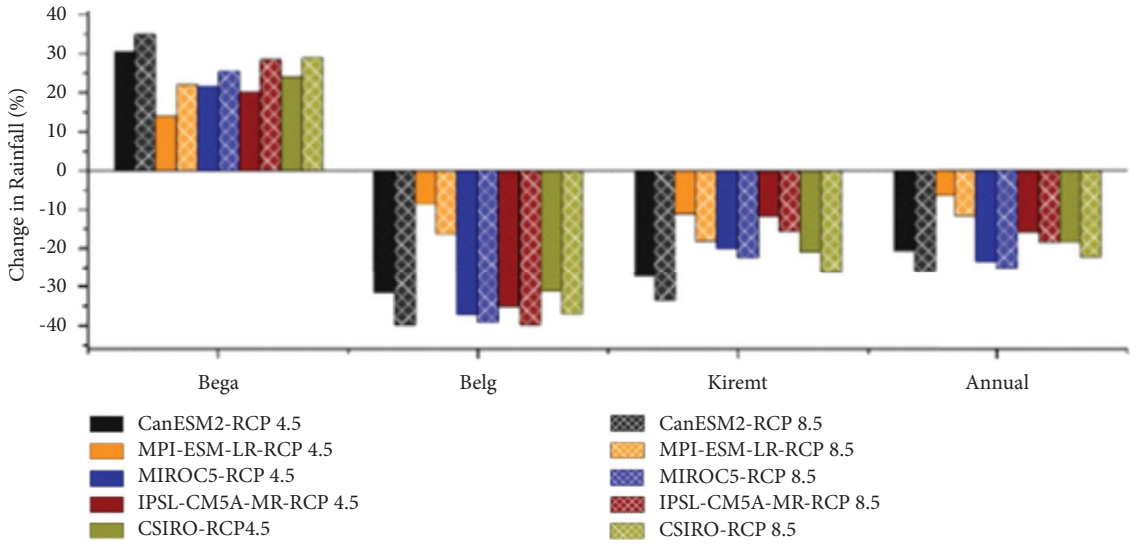

(a)

Figure 14: Continued.

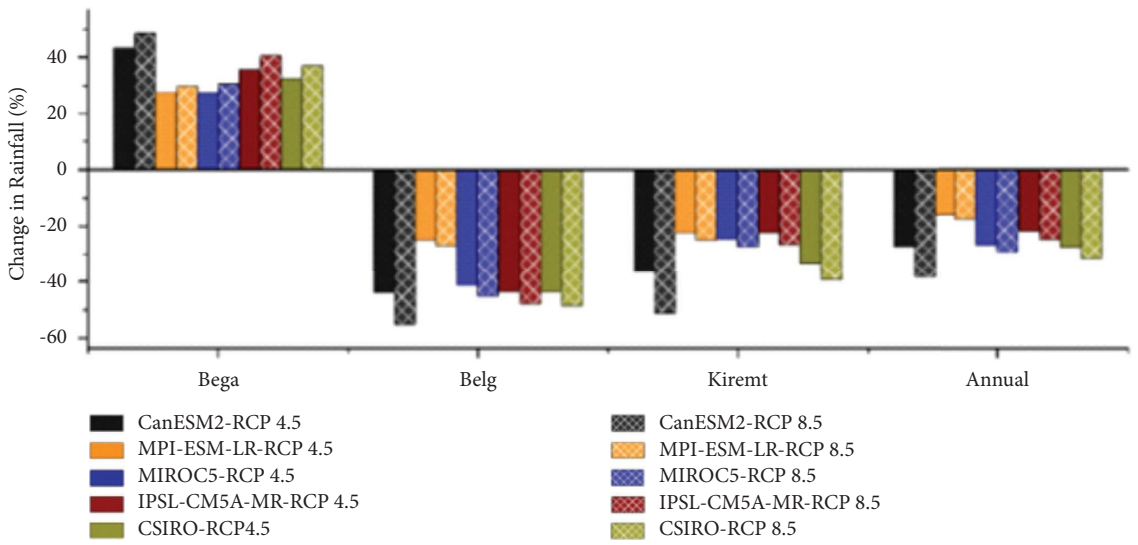

(b)

Figure 14: Percentage changes in annual and seasonal rainfall with reference to the baseline for (a) the near future period from 2021 to 2050 and (b) the far future period from 2071 to 2100.

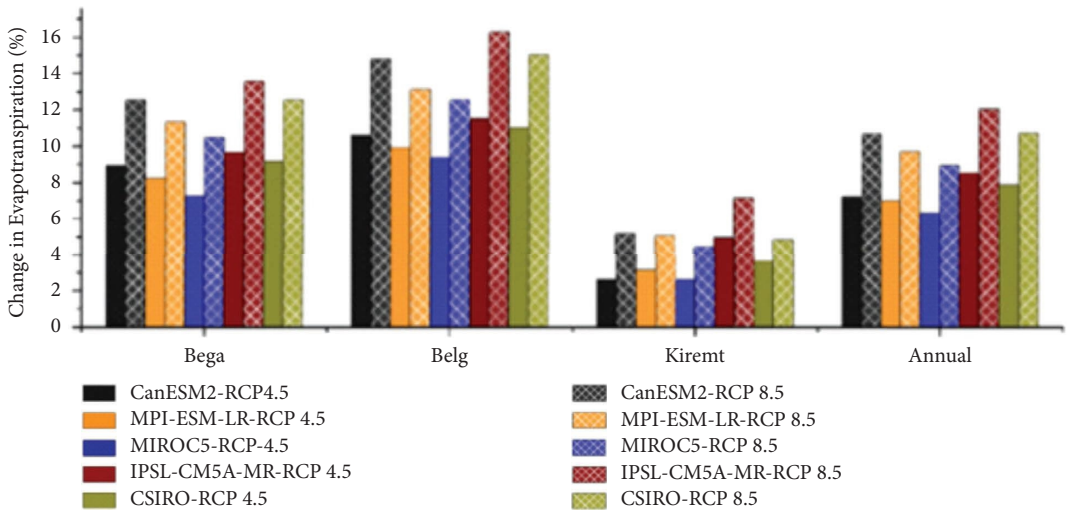

(a)

Figure 15: Continued.

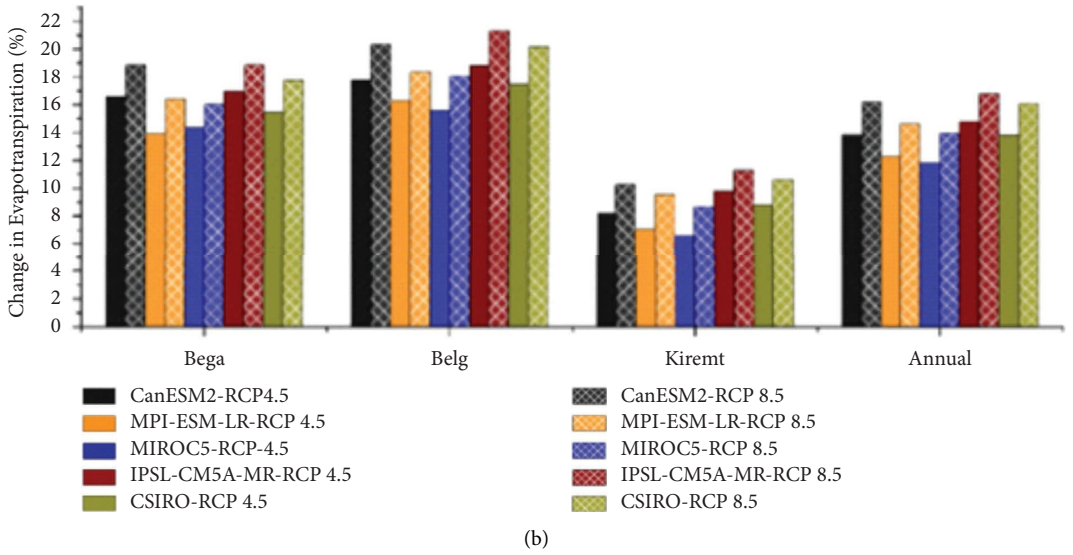

(b)

Figure 15: Percentage changes of annual and seasonal evapotranspiration with reference to the baseline in the (a) near future period from 2021 to 2050 and (b) far future period from 2071 to 2100.

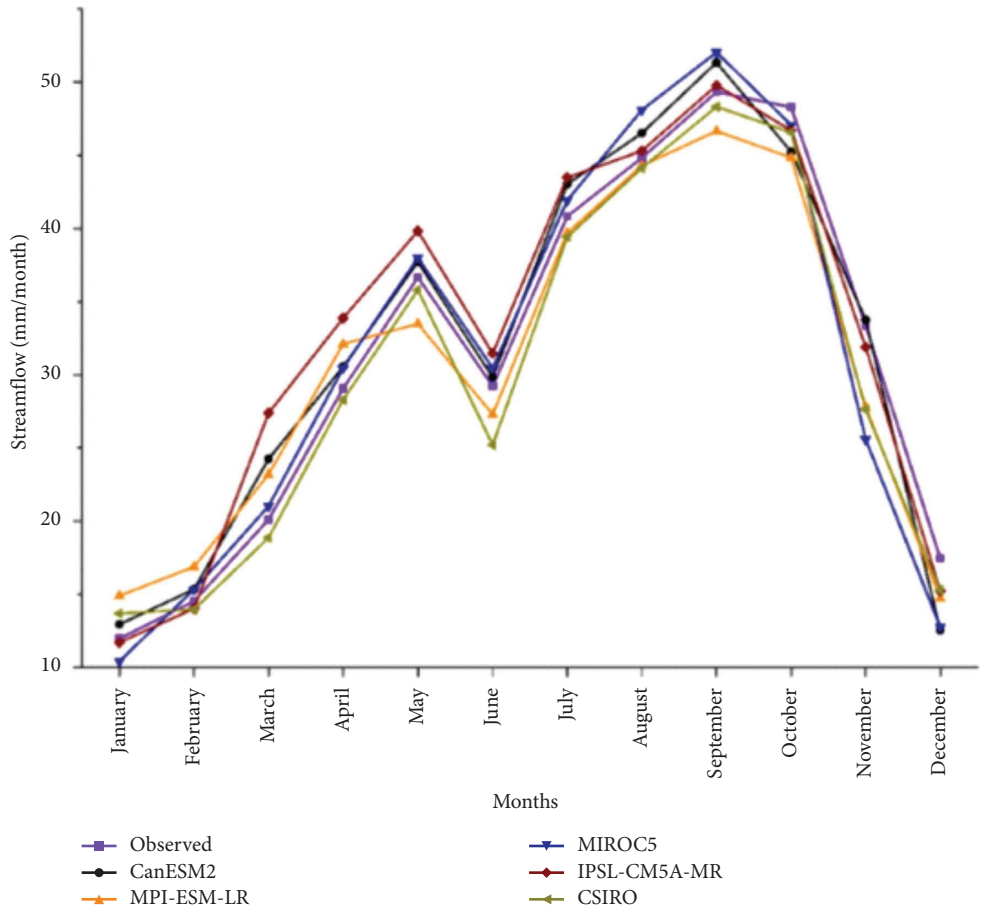

Figure 16: Observed and GCM simulated monthly streamflows in the baseline (1986–2005) period.

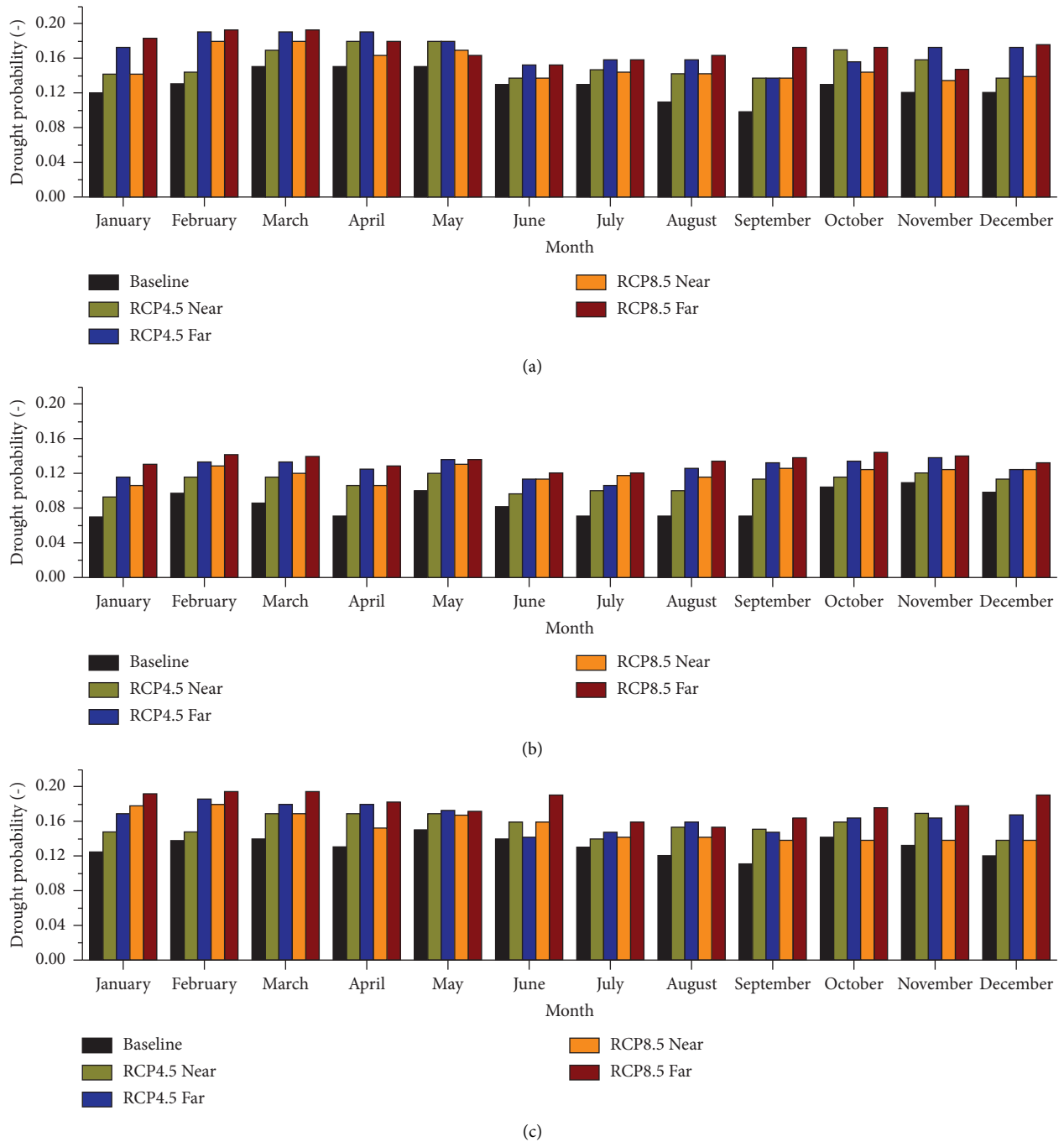

Figure 17: Probability of drought. (a) SPI; (b) SDI; and (c) RDI for the baseline and future periods.

a decline tendency. The relative change in average yearly precipitation is greater in RCP 8.5 than in RCP 4.5. The average annual precipitation change in the 2050s is expected to be between −37.2% and +33.1% for RCP 4.5 and between −38.2% and +63.2% for RCP 8.5 (Figure 20).

During the Belg and Bega seasons, simulations from five models including the chosen RACMO22T model show decreasing precipitation across the Hare catchment, while the remaining two models show higher precipitation. In the study region, estimates commencing four models, counting

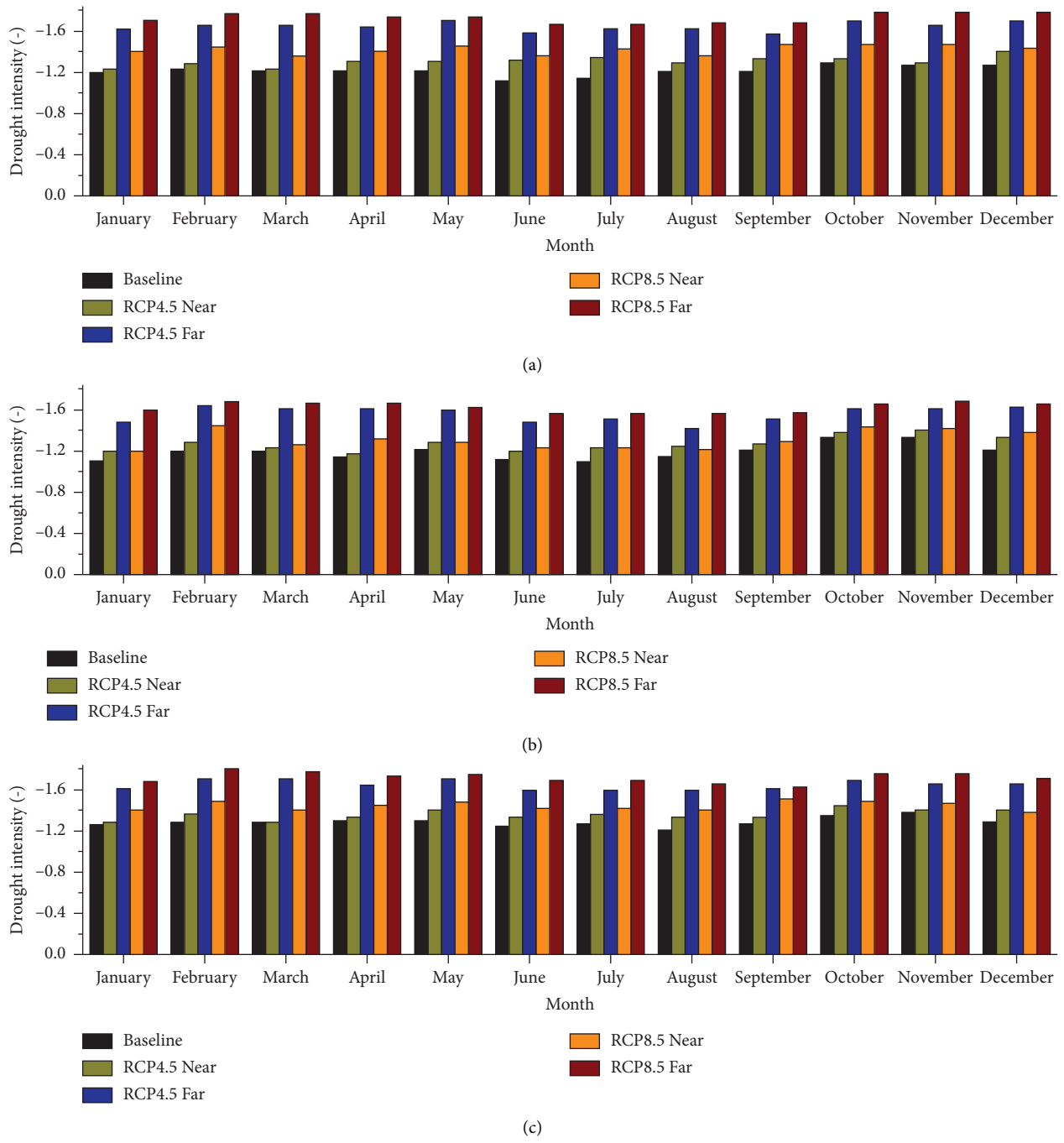

Figure 18: Mean drought intensities for the baseline and upcoming periods. (a) SPI, (b) SDI, and (c) RDI.

the selected RACMO22T model, show increasing precipitation, while the remaining three models show decreasing precipitation. The expected mean seasonal rainfall variations for Bega and Belg seasons are from −71.5% to 67% and from −69% to −8.5%, respectively. The predicted variations in average periodical rainfall for the Kiremt season range from −35% to 65%. Rainfall in the three seasons (Bega, Kiremt, and Belg) will likely vary by −18.1%, −0.023%, and −26.4%, on average and its approachable in value with the study [38].

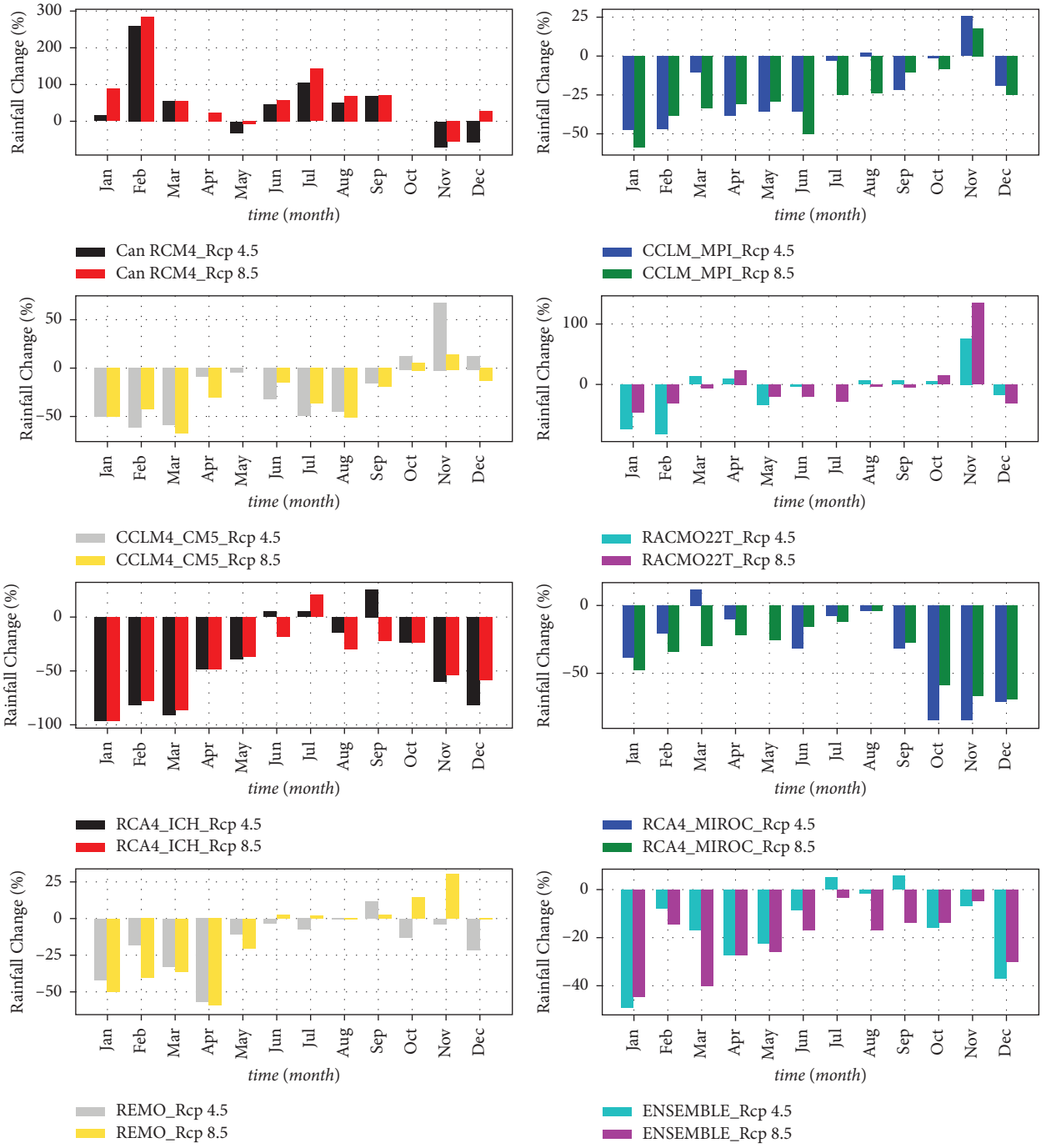

Figure 19: Projected change in monthly rainfall of the Hare river basin for the medium-term future (2051–2080) compared to the reference period (1986–2015) under the RCP4.5 and RCP8.5 scenarios.

With a few exceptions, rainfall simulations from most RCMs under RCP 8.5 indicate a steady drop intended for entire periods. For the Bega and Belg seasons, the estimated decreases in mean seasonal rainfall changes range from −68.6% to 87.4% for RCP 4.5 and from −59.6% to 15.5% for RCP 8.5, respectively, and similar study is conducted by [32]. Climate models predict a range of −12.1%–1.33% in mean seasonal rainfall for the Kiremt season. The average quantity

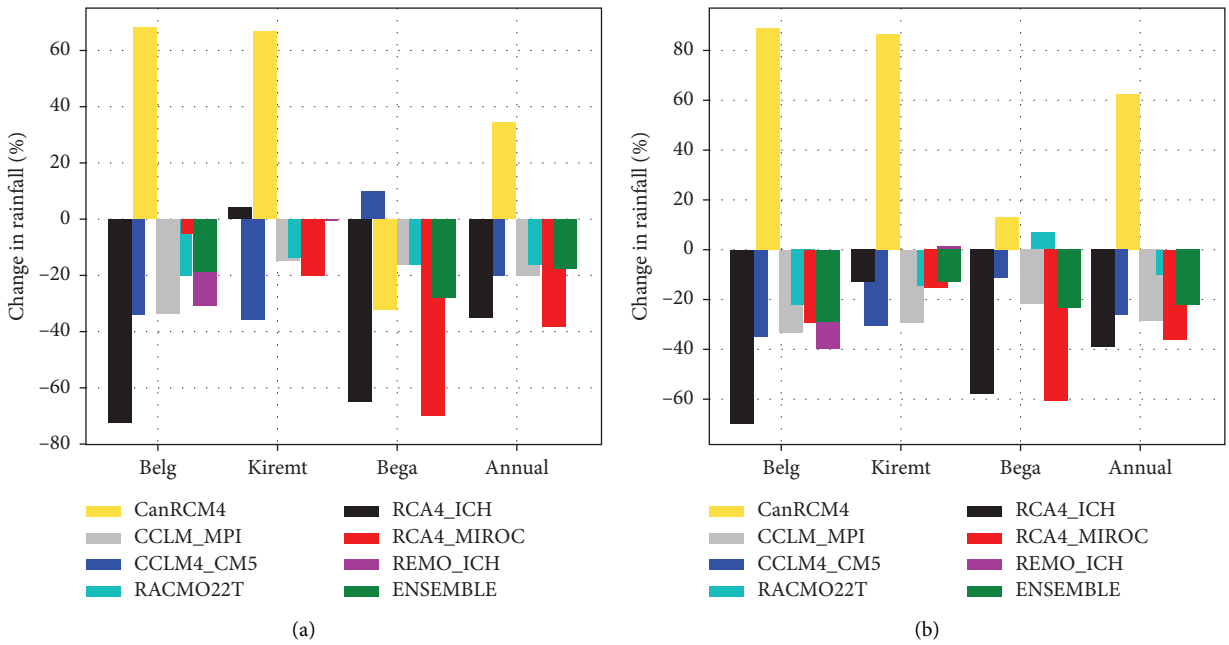

Figure 20: Change in mean seasonal and annual precipitation in the midterm future (2041–2070) compared to the reference period (1976–2005) under the RCP4.5 and RCP8.5 scenarios. (a) RCP4.5. (b) RCP8.5.

of average periodic precipitation will likely fall by a certain amount for Belg, Kiremt, and Bega seasons as 28.2%, 12.0%, and 22.6%, respectively.

4. Conclusion

Except for the CanRCM4 model, almost all RCMs indicated a considerable decline in average annual rainfall and stream flow. The CanRCM4 model simulation of rainfall in the Hare catchment differs dramatically from all other models. This might be ascribed to its unfortunate presentation in the study area, which could be linked to structural discrepancies in RCMs and process parameterization. For both climate emission scenarios, the mean yearly rainfall would be decreased from 16.7% to 10.2%. This study's expected outcomes are reliable through further scientific researches in the catchment. The study is crucial for rain-fed agriculture, management of reservoir storage and further water-related activities. Throughout general, maximum temperature, lowest temperature, and potential evapotranspiration exhibit reasonably consistent trends throughout the project region, whereas predicted rainfall shows significantly less consistency and volatility. Moreover, three drought indices SPI, SDI, and RDI are also used to examine how climate change affects drought aspects. The results show that future droughts will be more severe and protracted than the baseline era (under both emission scenarios). Residents of the Hare catchment depend greatly on the provision of runoff that found in natural waterways and periodic streams, that is negatively impacted by absence of rainfall brought on by climate change. Significant courtesy must be given to adopting new and problem solving mechanisms which is safe to climate alteration to preserve viable agricultural production and food for the future generation.

Data Availability

The data used to support the study are available from the corresponding author upon request.

Conflicts of Interest

The author declares that there are no conflicts of interest.

Acknowledgments

The author would like to acknowledge the respective Gamo zone agricultural office for their important data delivery in data collection and data analysis phases.

Supplementary Materials

The data of the current research, which contains, precipitation, T_{min}, T_{max}, and T_{av}, and RH_{min}, RH_{max}, and RH_{av} for three metrological stations were collected for the same period. Moreover, the overall output of the spatial and temporal data is presented in figure and tables. (*Supplementary Materials*)

References

[1] B. Malekmohammadi, C. B. Uvo, N T. Moghadam, R. Noori, and S. Abolfathi, "Environmental Environmental Risk Assessment of Wetland Ecosystems Using Bayesian Belief Networksisk assessment of wetland ecosystems using bayesian belief networks," *Hydrology*, vol. 10, no. 1, p. 16, 2023.

[2] M. Mahdian, M. Hosseinzadeh, S. Siadatmousavi et al., "Modelling impacts of climate change and anthropogenic activities on inflows and sediment loads of wetlands: case

study of the Anzali wetland," *Scientific Reports*, vol. 13, no. 1, p. 5399, 2023.

[3] R. Noori, M. Maghrebi, and S. Jessen, "Decline in Iran's groundwater recharge," *Research Square*, 2023.

[4] J. Agyekum, T. Annor, B. Lamptey, E. Quansah, and R. Y. K. Agyeman, "Evaluation of CMIP5 global climate models over the Volta Basin: precipitation," *Advances in Meteorology*, vol. 2018, Article ID 4853681, pp. 1–24, 2018.

[5] A. A. Akinsanola, V. O. Ajayi, A. T. Adejare et al., "Evaluation of rainfall simulations over West Africa in dynamically downscaled CMIP5 global circulation models," *Theoretical and Applied Climatology*, vol. 132, no. 1–2, pp. 437–450, 2017.

[6] U. Akumaga and A. Tarhule, "Projected changes in intra-season rainfall characteristics in the Niger river basin, west Africa," *Atmosphere*, vol. 9, no. 12, pp. 1983–1985, 2018.

[7] M. M. Alemu and G. T. Bawoke, "Analysis of spatial variability and temporal trends of rainfall in Amhara Region, Ethiopia," *Journal of Water and Climate Change*, vol. 11, no. 4, pp. 1505–1520, 2019.

[8] B. Ampadu, "Overview of hydrological and climatic studies in Africa: the case of Ghana," *Cogent Engineering*, vol. 8, no. 1, 2021.

[9] T. Annor, B. Lamptey, S. Wagner et al., "High-resolution long-term WRF climate simulations over Volta Basin. Part 1: validation analysis for temperature and precipitation," *Theoretical and Applied Climatology*, vol. 133, no. 3-4, pp. 829–849, 2017.

[10] A. Asfaw, B. Simane, A. Hassen, and A. Bantider, "Variability and time series trend analysis of rainfall and temperature in northcentral Ethiopia: A case study in Woleka sub-basin," *Weather and Climate Extremes*, vol. 19, pp. 29–41, 2018.

[11] A. Ayanlade, M. Radeny, J. F. Morton, and T. Muchaba, "Rainfall variability and drought characteristics in two agro-climatic zones: an assessment of climate change challenges in Africa," *Science of the Total Environment*, vol. 630, pp. 728–737, 2018.

[12] H. M. Badjana, P. Selsam, K. Wala et al., "Assessment of land-cover changes in a sub-catchment of the Oti basin (West Africa): A case study of the Kara River basin," *Zentralblatt für Geologie und Paläontologie, Teil I*, vol. 2014, no. 1, pp. 151–170, 2014.

[13] J. Balist, B. Malekmohammadi, H. R. Jafari, A. Nohegar, and D. Geneletti, "Detecting land use and climate impacts on water yield ecosystem service in arid and semi-arid areas. A study in Sirvan River Basin-Iran," *Applied Water Science*, vol. 12, no. 1, pp. 4–14, 2022.

[14] E. Bessah, A. O. Raji, O. J. Taiwo, S. K. Agodzo, and O. O. Ololade, "The impact of varying spatial resolution of climate models on future rainfall simulations in the Pra River Basin (Ghana)," *Journal of Water and Climate Change*, vol. 11, no. 4, pp. 1263–1283, 2020.

[15] A. Chemura, B. Schauberger, and C. Gornott, "Impacts of climate change on agro-climatic suitability of major food crops in Ghana," *PLoS One*, vol. 15, no. 6, pp. e0229881–21, 2020.

[16] M. Dembélé and S. J. Zwart, "Evaluation and comparison of satellite-based rainfall products in Burkina Faso, West Africa," *International Journal of Remote Sensing*, vol. 37, no. 17, pp. 3995–4014, 2016.

[17] M. Dembélé, B. Schaefli, N. van de Giesen, and G. Mariéthoz, "Suitability of 17 gridded rainfall and temperature datasets for large-scale hydrological modelling in West Africa," *Hydrology and Earth System Sciences*, vol. 24, no. 11, pp. 5379–5406, 2020.

[18] I. Pujiastuti and E. Nurjani, "Rainfall pattern variability as climate change impact in The Wallacea Region," *IOP Conference Series: Earth and Environmental Science*, vol. 148, Article ID 12023, 2018.

[19] B. Yisehak, "Prediction of flood frequency under a changing climate, the case of Hare watershed, Rift Valley Basin of Ethiopia," *Sustainable Water Resources Management*, vol. 7, no. 1, p. 9, 2021.

[20] D. Kwawuvi, D. Mama, S. K. Agodzo et al., "Spatiotemporal variability and change in rainfall in the oti river basin, west Africa," *Journal of Water and Climate Change*, vol. 13, no. 3, pp. 1151–1169, 2022.

[21] S. Gebrechorkos, S. Hülsmann, and C. Bernhofer, "Long-term trends in rainfall and temperature using high-resolution climate datasets in East Africa," *Scientific Reports*, vol. 9, no. 1, Article ID 11376, 2019.

[22] N. Alahacoon, M. Edirisinghe, M. Simwanda, E. Perera, V. Nyirenda, and M. Ranagalage, "Rainfall Rainfall Variability and Trends over the African Continent Using TAMSAT Data (1983–2020): Towards Climate Change Resilience and Adaptationariability and trends over the african continent using TAMSAT data (1983–2020): towards climate change resilience and adaptation," *Remote Sensing*, vol. 14, no. 1, p. 96, 2021.

[23] N. Arnell, J A. Lowe, A. J. Challinor, and T. J. Osborn, "Global and regional impacts of climate change at different levels of global temperature increase," *Climatic Change*, vol. 155, no. 3, pp. 377–391, 2019.

[24] K. Zisopoulou, D. Zisopoulos, and D. Panagoulia, "Water Water Economics: An In-Depth Analysis of the Connection of Blue Water with Some Primary Level Aspects of Economic Theory Iconomics: an in-depth analysis of the connection of blue water with some primary level aspects of economic theory I," *Water*, vol. 14, no. 1, p. 103, 2022.

[25] Y.-A. Liou and G. M. Mulualem, "Spatio–temporal Spatio–temporal Assessment of Drought in Ethiopia and the Impact of Recent Intense Droughtsssessment of drought in Ethiopia and the impact of recent intense droughts," *Remote Sensing*, vol. 11, no. 15, p. 1828, 2019.

[26] H. Ayele, M H. Li, C.-P. Tung, and T.-M. Liu, "Impact of Impact of Climate Change on Runoff in the Gilgel Abbay Watershed, the Upper Blue Nile Basin, Ethiopialimate change on runoff in the gilgel abbay catchment, the upper blue nile basin, Ethiopia," *Water*, vol. 8, no. 9, p. 380, 2016.

[27] B. T. Lambe and S. Kundapura, "Analysis of meteorological variability and tendency over Bilate basin of Rift Valley Lakes basins in Ethiopia," *Arabian Journal of Geosciences*, vol. 14, pp. 1–22, 2021.

[28] G. Girmay, A. Moges, and A. Muluneh, "Assessment of Assessment of Current and Future Climate Change Impact on Soil Loss Rate of Agewmariam Watershed, Northern Ethiopiaurrent and future climate change impact on soil loss rate of agewmariam catchment, northern Ethiopia," *Air, Soil and Water Research*, vol. 14, Article ID 117862212199584, 2021.

[29] M. Taye, E. Dyer, F. A. Hirpa, and K. Charles, "Climate Climate Change Impact on Water Resources in the Awash Basin, Ethiopiahange impact on water resources in the awash basin, Ethiopia," *Water*, vol. 10, no. 11, p. 1560, 2018.

[30] M. Tadese, L. Kumar, and R. Koech, "Long-Long-Term Variability in Potential Evapotranspiration, Water Availability and Drought under Climate Change Scenarios in the Awash River Basin, Ethiopiaerm variability in potential evapotranspiration, water availability and drought under

climate change scenarios in the awash river basin, Ethiopia," *Atmosphere*, vol. 11, no. 9, p. 883, 2020.

[31] S. Jang, M. L. Kavvas, K. Ishida et al., "A performance evaluation of dynamical downscaling of precipitation over Northern California," *Sustainability*, vol. 9, no. 8, p. 1457, 2017.

[32] T. Mana, B. W. Abebe, and S. D. Hatiye, "Effect of climate change on reservoir water balance and irrigation water demand: a case of Gidabo irrigation project, Rift Valley Basin, Ethiopia," *Environmental Monitoring and Assessment*, vol. 195, no. 7, p. 866, 2023.

[33] E. Mutayoba and J. J. Kashaigili, "Evaluation for the performance of the CORDEX regional climate models in simulating rainfall characteristics over Mbarali river catchment in the Rufiji basin, Tanzania," *Journal of Geoscience and Environment Protection*, vol. 5, no. 4, pp. 139–151, 2017.

[34] T. F. Negewo and A. K. Sarma, "Estimation of water yield under baseline and future climate change scenarios in Genale watershed, Genale Dawa river basin, Ethiopia, using SWAT model," *Journal of Hydrologic Engineering*, vol. 26, no. 3, Article ID 5020051, 2021.

[35] Y. A. Orke and M. H. Li, "Impact of climate change on hydrometeorology and droughts in the Bilate watershed. Ethiopia," *Water*, vol. 14, no. 5, p. 729, 2022.

[36] M. T. Taye, E. Dyer, F. A. Hirpa, and K. Charles, "Climate change impact on water resources in the Awash basin. Ethiopia," *Water*, vol. 10, no. 11, p. 1560, 2018.

[37] A. W. Worako, A. T. Haile, and M. T. Taye, "Implication of bias correction on climate change impact projection of surface water resources in the Gidabo sub-basin, Southern Ethiopia," *Journal of Water and Climate Change*, vol. 13, no. 5, pp. 2070–2088, 2022.

[38] Y. Yira, B. Diekkrüger, G. Steup, and A. Y. Bossa, "Impact of climate change on hydrological conditions in a tropical West African catchment using an ensemble of climate simulations," *Hydrology and Earth System Sciences*, vol. 21, no. 4, pp. 2143–2161, 2017.